METALLURGY AND FOUNDRY ENGINEERING – Vol. 31, 2005, No. 2

Edward Fraś*, Marcin Górny**, Hugo F. López***

EUTECTIC TRANSFORMATION IN DUCTILE CAST IRON. PART I – THEORETICAL BACKGROUND

SYMBOLS

Symbols	Meaning	Definition	Units
a	Material mould ability to absorb of heat	$a = \sqrt{k_m c_m}$	J/(cm^2·ºC·s$^{1/2}$)
A	Parameter	Eq. (10)	s$^{1/2}$/m
b	Nucleation coefficient of graphite	Eq. (58)	^{o}C
B	Temperature parameter	Eq. (14)	–
c	Specific heat of metal	Table 1	J/(cm^3·ºC)
c_m	Specific heat of mould material	–	J/(cm^3·ºC)
C	Carbon content in cast iron	–	wt. %
C_e	Carbon content in graphite eutectic	Eq. (2)	wt. %
CT	Chilling tendency	Eqs. (67), (68)	s$^{1/2}$/ºC$^{1/3}$
C_2, C_3, C_4, C_{gr}	Carbon content in austenite, liquid and graphite	Fig (3b)	wt. %
D	Diffusivity of carbon in austenite	Eq. (64)	cm^2/s
f_{gr}	Fraction of pre-eutectic graphite	Eq. (1)	–

* Prof., ** Ph.D., Faculty of Foundry Engineering, AGH University of Science and Technology, Cracow, Poland; edfras@agh.edu.pl; mgorny@agh.edu.pl, ** Author is an award holder of the NATO Science Fellowship Programme

*** Prof., Department of Materials Engineering, University of Wisconsin-Milwaukee, P.O. Box 784, Milwaukee, WI 53201, USA; hlopez@uwm.edu

F_c	Surface area of the casting	–	cm^2
F_{ch}	Half surface area chill triangle	Figure11	cm^2
k	Coefficient	Eqs. (39), (43)	
k_m	Heat conductivity of the mould material	–	J/(s·cm·ºC)
l_s	Size of substrate for nucleation of graphite	–	cm
$\langle l \rangle$	Mean size of substrates for nucleation of graphite	–	cm
L_e	Latent heat of graphite eutectic	Table 1	J/cm^3
m_{gr}	Mass of graphite	Eq. (31)	g
m_l	Mass of graphite in liquid	Eq. (30)	g
m_γ	Mass of graphite in austenite	Eq. (35)	g
M	Casting modulus	Eqs. (11), (52), (55)	cm
M_{cr}	Critical casting modulus	Eq. (70)	cm
N	Volumetric nodule count	Eqs. (57), (62)	cm^{-3}
N_s	Density of substrates for nucleation of graphite	–	cm^{-3}
P_{cr}	Coefficient	Eq. (66)	$(cm\cdot{}^oC^{1/3})/s^{1/2}$
P	Phosphorus content in cast iron	–	wt. %
q_a	Accumulated heat flux in casting	Eq. (6)	J/s
q_m	Heat flux extracted from casting into mould casting	Eq. (5), (50)	J/s
q_s	Heat flux generated during solidification	Eq. (7),(49)	J/s
Q	Metal cooling rate	Eq. (15)	ºC/s
R_1	Graphite nodule radius	Figure 3b	cm
R_2	Outer radius of austenite envelope	Figure 3b	cm
R_{2m}	Austenite envelope radius at maximum undercooling	Eq. (47)	cm
s	Wall thickness	–	cm
s_{cr}	Critical wall thickness	Eqs. (71), (72)	cm
Si	Silicon content in cast iron	–	wt. %

t	Time	–	s
t_m	Time at the maximum undercooling	Eq. (21)	s
t_s	Time at the onset of graphite eutectic solidification	–	s
T	Temperature	–	ºC
T_c	Equilibrium temperature of the cementite eutectic	Table 1	ºC
T_i	Initial temperature of metal in mould cavity	–	ºC
T_m	Temperature at maximum undercooling of graphite eutectic	Figure 2a	ºC
T_p	Pouring temperature	–	ºC
T_s	Equilibrium temperature of the graphite eutectic	Table 1	ºC
V_c	Volume of casting	–	cm^3
z	Parameter	Eq. (54)	–
α	Wedge angle	Figure 11	o
α_d	Thermal diffusivity of mould material	k_m/c_m	cm^2/s
β	Coefficient	Table 1	$^oC^{-1}$
ΔH	Enthalpy of metal	–	J/cm^3
ΔT	Undercooling of graphite eutectic	–	
ΔT_m	Maximum undercooling of graphite eutectic	$\Delta T_m = T_s - T_m$	ºC
ΔT_{sc}	Range of temperature, $\Delta T_{sc} = T_s - T_c$	Table 1	ºC
θ	Wetting angle between substrate and nuclei of graphite	–	o
ρ_l	Density of melt	Table 1	g/cm^3
ρ_{gr}	Density of graphite	Table 1	g/cm^3
ρ_γ	Density of austenite	Table 1	g/cm^3
σ	Interfacial energy between the nucleus and the melt	–	J/cm^2
φ, φ_1	Parameters	Eqs. (25), (26)	%
ω	Frequency	Eq. (17)	1/s

1. INTRODUCTION

Ductile cast iron is a modern engineering material whose production is continually increasing. Hence, there are numerous reports related to the production of nodular cast iron, some of which are of essential importance as they are linked to the solidification kinetics. In ductile cast iron, solidification is closely related to the nucleation and growth of nodular graphite. Yet, nucleation is the dominant process at the onset of solidification and it establishes the final nodule count. Accordingly, increasing the nodule count in a given cast iron leads to:

- Increasing strength and ductility in ductile cast iron [1].
- Reduction of microsegregation of alloying elements [2, 3], and improving microstructural homogeneity. Here, the type of eutectic transformation (stable or metastable) is also influenced due to the re-distribution of alloying elements.
- Reduction in the chilling tendency of cast iron [4, 5].
- Increasing pre-shrinkage expansion [6].
- Increasing formation of open and closed contraction cavity volumes [7].
- Increasing fraction of ferrite in the microstructure [8].

The chilling tendency (CT) of cast iron dictates their subsequent performance in diverse applications. In particular, cast iron possessing a high chilling tendency is prone to develop zones of white or mottled iron. Considering that, these regions can be extremely hard, their machinability can be severely impaired. Alternatively, if white iron is the desired structure a relatively small chilling tendency favours the formation of grey iron. This in turn leads to poor hardness and wear properties for the cast components. Hence, considerable efforts have been made in correlating various factors of technological relevance (inoculation practice, iron composition, pouring temperature, etc.) with the chill of cast iron.

In this work, a simple analytical model of eutectic transformation in ductile cast iron is proposed. The model enables the determination of nodule counts in nodular cast iron, the chilling tendency CT and chill of ductile cast iron.

2. ANALYSIS

Ductile cast iron is often hypereutectic, where the volume fraction of pre-eutectic graphite f_{gr} is given by

$$f_{gr} = \frac{\rho_l \left(\mathrm{C} - \mathrm{C_e}\right)}{100\ \rho_{\mathrm{gr}} - \mathrm{C_e}\rho_l + \mathrm{C}(\rho_l - \rho_{gr})} \tag{1}$$

where $\mathrm{C_e} = 4.26 - 0.30\mathrm{Si} - 0.36\mathrm{P}$ (2)

The influence of carbon and silicon on the pre-eutectic volume fraction of graphite is shown in Figure 1. From this figure it can be observed that for a useful C and Si range in the

foundry practice f_{gr} ranges from 0 to 0.02; as a result, solidification of pre-eutectic graphite can be neglected.

In this case, during solidification, heat extraction leads to changes in the relative energies of solid and liquid in two ways:

1) a reduction in the enthalpy of the liquid or solid due to cooling given by $\Delta H = \int cdT$,
2) a release heat of the eutectic solidification through the enthalpy contribution, known also as the latent heat (L).

Hence, the heat transfer process can be described by the heat balance equation

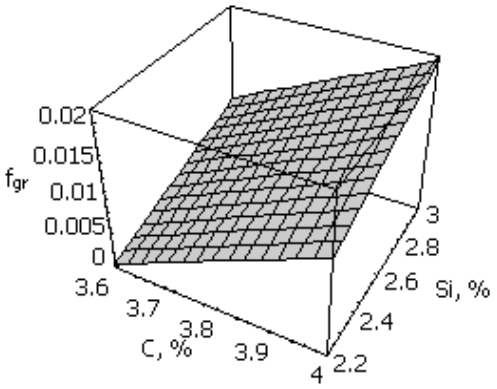

Fig. 1. *Effect of carbon and silicon on the volumetric fraction of pre-eutectic graphite in hypereutectic cast iron*

$$q_m = q_s + q_a \tag{3}$$

Heat transfer during solidification can be very complex and analytical solutions are not always available, so numerical methods are commonly employed. However, in sand castings, heat transfer is mainly determined by the properties of the sand mold as shown by Chvorinov [9].

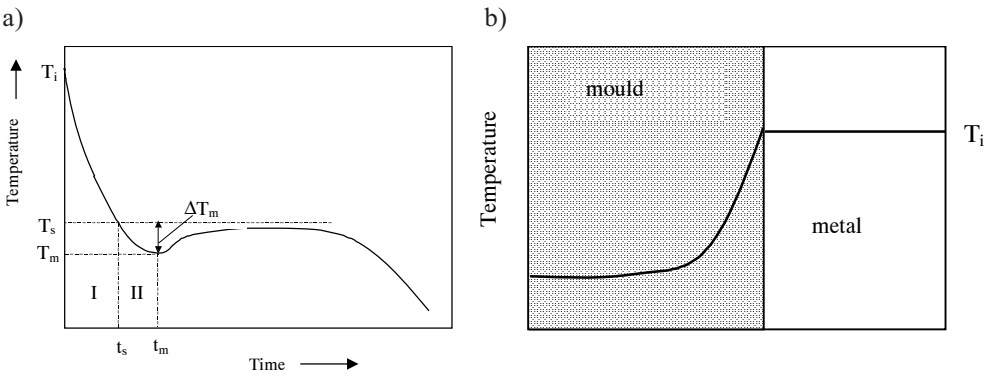

Fig. 2. *Cooling curve for eutectic ductile cast iron (a) and temperature profile in the mold-metal system (b)*

Figure 2b shows the ideal temperature profile expected for sand-mould metal systems. The heat flux going into the mold can be described by

$$q_m = \frac{T\ k_m}{\sqrt{\pi\ \alpha_d\ t}} \tag{4}$$

Taking into account the thermal diffusivity $\alpha_d = k_m/c_m$ and the surface area F_c of the casting, Eq. (4) can be rearranged as

$$q_m = \frac{a\, F_c T}{\sqrt{\pi\, t}} \tag{5}$$

where $a = \sqrt{k_m c_m}$.

The above expression neglects curvature effects associated with the metal-mold interface. Moreover, it is assumed that the temperature distribution along the metal is uniform. Hence, the accumulated heat flux in the metal can be described by

$$q_a = \frac{cV_c dT}{dt} \tag{6}$$

The heat flux q_s generated during solidification depends on the particular solidification mechanism and in the present work it can be described by

$$q_s = L_e N V_c \frac{dV}{dt} \tag{7}$$

where dV/dt is the volumetric solidification rate of eutectic cells (cm^3/s). During solidification, two main stages can be distinguished (Fig. 2a).

First Stage

In this stage, the temperature of the melt decreases from T_i to the equilibrium temperature for graphite eutetctic T_s with no solidification events (Fig. 2a). Accordingly, $q_s = 0$ and Eq. (3) can be rewritten as

$$q_m = q_a \tag{8}$$

Taken into consideration Eqs. (5) and (6) and solving Eq. (8) for the initial conditions: $T = T_i$ at $t = 0$, the temperature during this stage is given by

$$T = T_i \exp\left(-\frac{\sqrt{t}}{A\, M}\right) \tag{9}$$

where:

$$A = \frac{c\,\sqrt{\pi}}{2\, a} \tag{10}$$

$$M = \frac{V_c}{F_c} \tag{11}$$

Differentiating Eq. (9) yields an equation for the cooling rate as

$$\frac{dT}{dt} = -\frac{T_i}{2A\,M\,\sqrt{t}} \exp\left(-\frac{\sqrt{t}}{A\,M}\right) \tag{12}$$

For $t = t_s$, $T = T_s$, and the time elapsed during the first stage can be found from Eq. (9)

$$t_s = (A\,B\,M)^2 \tag{13}$$

where

$$B = \ln\frac{T_i}{T_s} \tag{14}$$

The metal cooling rate at the end of first stage can be calculated by taking into account Eqs. (12)–(14) for $t = t_s$, $T = T_s$ condition and after rearranging, yielding[1)]

$$\frac{dT}{dt} = Q = \frac{2\,T_s\,a^2}{\pi\,B\,c^2\,M^2} \tag{15}$$

Second Stage

During this stage, the solidification of graphite eutectic occurs in the $t_s < t < t_m$ time range or in the $T_s < T < T_m$ temperature range (Fig. 2a). The initial segment of the cooling curve where the eutectic transformation takes place can be defined as a function of the degree of maximum undercooling $\Delta T_m = T_s - T_m$ (Fig. 2a). The solidification temperature for this temperature range can be described by [10]

$$T = T_s - \Delta T_m \sin\,\omega(t - t_s) \tag{16}$$

where

$$\omega = \frac{\pi}{2(t_m - t_s)} \tag{17}$$

Equation (16) is of empirical nature. However it has been shown to provide an excellent description of the experimental outcome [10]. Accordingly, during second stage the cooling rate can be found by differentiating Eq. (16).

$$\frac{dT}{dt} = -\Delta T_m \omega \cos[\omega(t - t_s)] \tag{18}$$

[1)] It is assumed that cooling rate has positive sign.

Therefore at the beginning of stage II when $t = t_s$, cos0 = 1, the cooling rate can be described by[2)]

$$Q = \frac{dT}{dt} = \omega \, \Delta T_m \tag{19}$$

Combining Eqs. (17) and (19), and rearranging, yields

$$\frac{\Delta T_m}{(t_m - t_s)} = \frac{2}{\pi} Q \tag{20}$$

At the onset of eutectic solidification ($t = t_s$), the cooling rates in the first and second stages it can be assumed equal each other. Therefore, using Eqs. (13), (15), and (20), the time for the maximum undercooling can be determined from

$$t_m = \frac{\pi B \, c^2 \, M^2 \, (B \, T_s + \pi \, \Delta T_m)}{4 \, a^2 \, T_s} \tag{21}$$

Nuclei N of nodular graphite are formed in the casting volume of liquid V_c, and from each nucleus rise a single eutectic cell of spherical shape. Hence, the volume of the eutectic cell with radius R_2 (Fig. 3b) is given by $V = (4 \, \pi \, R_2^3)/3$, while the differential volume increment is given by $dV = 4 \, \pi \, R_2^2 \, dR_2$. Accordingly, taking into account Eq. (7) the expression for the rate of heat generation can be described by

$$q_s = \frac{4 \, \pi \, L_e \, N \, V_c \, R_2^2 \, dR_2}{dt} \tag{22}$$

In order to determine the radius R_2, as well as the growth rate of the cell, dR_2/dt the eutectic transformation in nodular cast iron will now be considered. Taking into account diffusional transport during the eutectic transformation and assuming spherical geometry (Fig. 3), the steady state solution for carbon diffusion through the austenite shell can be defined by solving equation

$$D\left(\frac{2}{r}\frac{d\mathrm{C}}{dr} + \frac{d^2\mathrm{C}}{dr^2}\right) = 0 \tag{23}$$

[2)] It is assumed that cooling rate has positive sign.

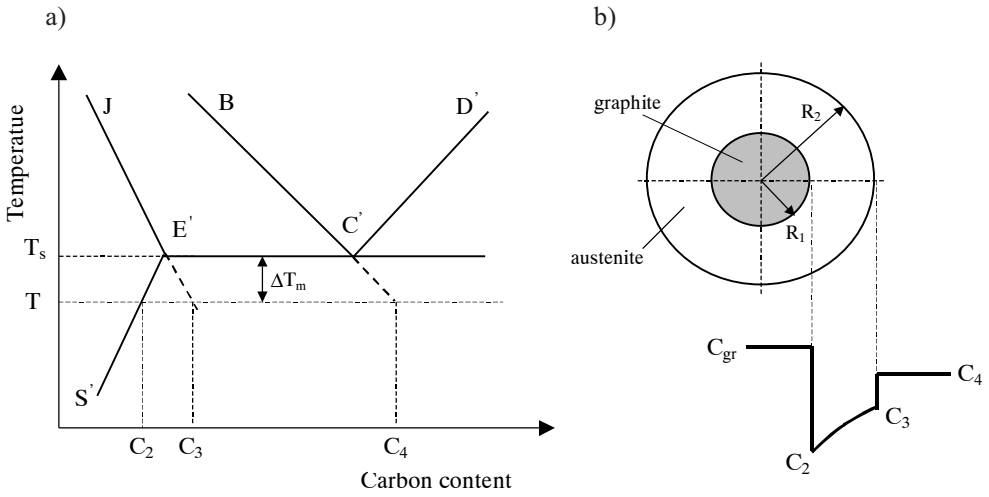

Fig. 3. *Schematic representation of a Fe-C phase diagram section (a) and corresponding carbon profile for a spherical eutectic cell (b)*

The general solution to the above equation yields

$$C = \varphi + \frac{\varphi_1}{r} \tag{24}$$

where r is the radial coordinate, $R_1 < r < R_2$ and φ and φ_1 are constants which can be determined from the boundary conditions: $C = C_3$ at $r = R_2$ and $C = C_2$ at $r = R_1$. This yields:

$$\varphi = C_3 - \frac{R_1(C_2 - C_3)}{R_2 - R_1} \tag{25}$$

$$\varphi_1 = \frac{R_1 R_2 (C_2 - C_3)}{R_2 - R_1} \tag{26}$$

Hence, taking into account Eqs. (24), (26) the solute concentration profile in the austenite envelope can be described by:

$$C(r) = C_3 - \frac{R_1 (C_2 - C_3)(r - R_2)}{r\ (R_2 - R_1)} \tag{27}$$

Moreover, deriving Eq. (27) with respect to r yields the carbon concentration gradient in the austenite envelope at the liquid – austenite interface.

$$\frac{dC}{dr} = \frac{R_1\, R_2\ (C_2 - C_3)}{r^2 (R_1 - R_2)} \tag{28}$$

Also, at the austenite solidification interface $r = R_2$, the concentration gradient becomes

$$\frac{d\mathrm{C}}{dR_2} = -\frac{R_1(\mathrm{C}_3 - \mathrm{C}_2)}{R_2\left(R_2 - R_1\right)} \tag{29}$$

Introducing a mass balance in the diffusional system (Fig. 3b) where (C_4) is the carbon content in the volume $(4\pi R_2^3)/3$ prior to the eutectic transformation (when only liquid is the stable phase). In this case, the mass of carbon in the liquid can be given by

$$m_l = \frac{4}{3}\,\pi\, R_2^3\;\mathrm{C}_4 \tag{30}$$

After the eutectic transformation, the diffusional system is depicted by a graphite nodule of radius R_1 and concentration C_{gr} surrounded by an austenite envelope of radii R_1 and R_2. The mass of carbon in the graphite nodule can be determined from

$$m_{gr} = \frac{4}{3}\,\pi\, R_1^3\;\mathrm{C}_{gr} \tag{31}$$

A differential increment in the volume of the austenite envelope $dV = 4\pi r^2 dr$ causes a differential increment in the carbon mass according to

$$dm_\gamma = 4\,\pi\,\mathrm{C}(r)\,r^2 dr \tag{32}$$

Also, the carbon mass in the austenite envelope is described by

$$m_\gamma = 4\pi \int_{R_1}^{R_2} \mathrm{C}(r) r^2 dr \tag{33}$$

Considering Eqs. (27) and (33) and rearranging terms yields

$$m_\gamma = \frac{4}{3}\pi \left[\mathrm{C}_3 R_2^3 - \mathrm{C}_2 {R_1}^3 - \frac{1}{2} R_1\, R_2(\mathrm{C}_3 - \mathrm{C}_2)(R_2 + R_1)\right] \tag{34}$$

In the above equation, the third term within brackets is relatively small and can be neglected. This yields

$$m_\gamma = \frac{4}{3}\pi \left(\mathrm{C}_3 R_2^3 - \mathrm{C}_2 {R_1}^3\right) \tag{35}$$

From the mass balance ($m_l = m_{gr} + m_\gamma$), based on Eq. (30), (31) and (35) R_1 is found as

$$R_1 = R_2 \left(\frac{C_4 - C_3}{C_{gr} - C_2} \right)^{1/3} \tag{36}$$

In addition, the condition for continuity across the liquid – austenite interface needs to be taken into account. This condition using Fick law can be written as

$$(C_4 - C_3) \frac{dR_2}{dt} = D \frac{dC}{dR_2} \tag{37}$$

Combining Eqs. (29), (36), and (37) yields

$$R_2 dR_2 = kDdt \tag{38}$$

where

$$k = \frac{(C_3 - C_2)}{(C_4 - C_3)\left(\sqrt[3]{\frac{C_{gr} - C_2}{C_4 - C_3}} - 1 \right)} \tag{39}$$

The above expression can be correlated with the degree of undercooling, ΔT. Assuming that the JE′, E′S′ and BC′ lines for the Fe-C system (Fig. 3a) are straight the concentrations in Eq. (39) can be given by:

$$C_2 = C_{E'} - \frac{\Delta T}{m_2} \tag{40}$$

$$C_3 = C_{E'} + \frac{\Delta T}{m_3} \tag{41}$$

$$C_4 = C_{C'} + \frac{\Delta T}{m_4} \tag{42}$$

where: m_2 , m_3 and m_4 are the slopes of the solubility lines JE′, E′ S′ and BC′ respectively.

For Fe-C alloys the following values can be employed: $C_{C'} = 4.26\%$, $C_{E'} = 2.08\%$, $m_2 = 275\ ^{o}C / \%$, $m_3 = 189.6\ ^{o}C / \%$, and $m_4 = 113.2\ ^{o}C / \%$. Using this data, estimations of k values are plotted in Figure 4. From this figure, it is apparent that k tends to exhibit a linear trend with ΔT. Accordingly, k can be described by

$$k = \beta\, \Delta T \tag{43}$$

where $\beta = 0.00155\ ^{o}C^{-1}$. Moreover, it can be shown that the effect of Si on β is negligible.

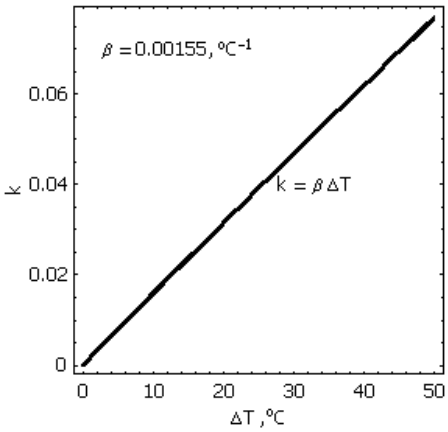

Fig. 4. *Graphic plot of Eq. (39) function as a function of the degree of undercooling, ΔT*

In addition, considering that the degree of undercooling $\Delta T = T_s - T$, from Eqs. (16), (38) and (43), it is found that

$$R_2\, dR_2 = \beta\, D\, \Delta T_m \sin\left[\omega\left(t - t_s\right)\right] dt \tag{44}$$

Hence, integrating the above expression for the limiting conditions $t = t_s$ at $R_2 = 0$, yields

$$R_2 = \left\{\frac{2\,\beta\, D\, \Delta T_m}{\omega}\left[1 - \cos\ \omega\left(t - t_s\right)\right]\right\}^{1/2} \tag{45}$$

Differentiating Eq. (45) with respect to time yields the rate of eutectic cell growth

$$\frac{dR_2}{dt} = \left\{\frac{\beta\, D\, \omega\, \Delta T_m}{2\,\left[1 - \cos\ \omega\left(t - t_s\right)\right]}\right\}^{1/2} \sin\left[\omega\left(t - t_s\right)\right] \tag{46}$$

Then, at the time $t = t_m$, and by taking into account Eq. (17), expressions for the cell radius, as well as the cell growth rate at the maximum undercooling are found:

$$R_{2,m} = \left(\frac{2\,\beta\, D\, \Delta T_m}{\omega}\right)^{1/2} \tag{47}$$

$$\frac{dR_{2,m}}{dt} = \left(\frac{\beta\, D\, \omega\, \Delta T_m}{2}\right)^{1/2} \tag{48}$$

In addition, by taking into account Eqs. (10), (13), (17), (21), (22), (47) and (48), the heat flux generated during solidification at the time $t = t_m$ is given by

$$q_s = 4\, L_e N\, V_c \frac{c\, M}{a} \left[\frac{B\, \Delta T_m \left(\pi\, \beta\, D\, \Delta T_m\right)^3}{T_s} \right]^{1/2} \tag{49}$$

Moreover, combining Eqs. (3) and (21) for the same time $t = t_m$, the heat flux going into the mold can be described by

$$q_m = \frac{2\, F_c\, a^2\, T_s^{3/2}}{\pi\, c\, M\, B^{1/2} \left(\pi\, \Delta T_m + T_s\, B\right)^{1/2}} \tag{50}$$

At $t = t_m$, the cooling rate is zero and as a consequence the rate of heat accumulation q_a is also zero. Hence, the heat balance equation (Eq. (3)) becomes

$$q_s = q_m \tag{51}$$

Finally, by taking into account Eqs. (11), (21), (49) and (51) an expression for the modulus of casting can be obtained.

$$M = \frac{a}{(D\beta)^{1/2}} \left(\frac{T_s^{\,2}}{2\, \pi^{5/2} B\, N\, L_e\, c^2\, \Delta T_m^2\, \left(\pi\, \Delta T_m + T_s B\right)^{1/2}} \right)^{1/3} \tag{52}$$

In nodular cast iron, the pouring temperature, T_p ranges from 1250 to 1450°C. Hence, taking into account that $T_p = T_i$, typical B values (Eq. (14)) range from 0.074 to 0.223. Figure 5 shows graphically the $\Delta T_m^2 \left(\pi\, \Delta T_m + T_s B\right)^{1/2}$ and $z\, \Delta T_m^2 T_s^{1/2}$ functions versus ΔT_m for two extreme values of B.

From this figure it is evident that

$$\Delta T_m^2 \left(\pi\ \Delta T_m + T_s\, B\right)^{1/2} \approx z\, T_s^{1/2}\, \Delta T_m^2 \tag{53}$$

where $z = 0.41 + 0.93B$ (54)

Accordingly, taking into account Eqs. (52) and (53), N can be simplified to the following form

$$M = a \left(\frac{T_s}{D\, \beta} \right)^{1/2} \left(\frac{1}{2\, \pi^{5/2} z\, B\, N\, L_e \Delta T_m^2} \right)^{1/3} \tag{55}$$

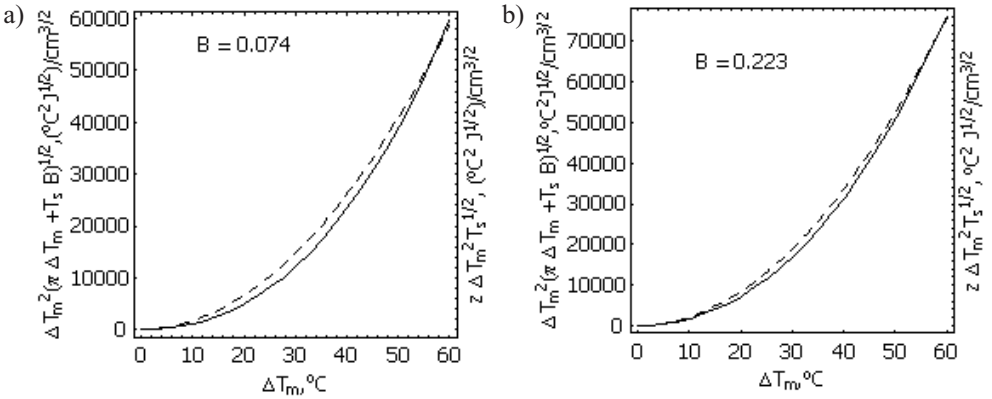

Fig. 5. *Influence of ΔT_m and B on the $\Delta T_m^2 \left(\pi\, \Delta T_m + B\, T_s\right)^{1/2}$ (solid line) and $z\ T_s^{1/2}\ \Delta T_m^2$ (dotted line) functions for: a) B = 0.074; b) B = 0.223*

3. NODULE COUNT

Eq. (55) can be rewritten as a function of the cooling rate (taking into account Eq. (15)) as

$$N = \frac{c\ B^{1/2}}{4\ 2^{1/2}\ \pi\, z\ L_e\ \Delta T_m^2} \left(\frac{Q}{D\ \beta} \right)^{3/2} \tag{56}$$

The nucleation of graphite during solidification is of heterogeneous nature, on preferential substrates of various sizes, l_s. The active substrate set is randomly distributed in the undercooled melt and it can be given by the substrate volume density, N_s. A simple heterogeneous nucleation model previously developed [11] is employed in this work. Accordingly, the volume density of graphite nodules can be given by

$$N = N_s \exp\left(-\frac{b}{\Delta T_m} \right) \tag{57}$$

where $b = \dfrac{4\ T_s\ \sigma\ \sin\theta}{L_e \left\langle l \right\rangle}$ (58)

Combining Eqs. (56) and (57) yields

$$N_s \exp\left(-\frac{b}{\Delta T_m} \right) = \frac{c\ B^{1/2}}{4\ \ 2^{1/2}\ \pi\, z\ \ L_e\ \ \Delta T_m^2} \left(\frac{Q}{D\ \beta} \right)^{3/2} \tag{59}$$

From this equation, the maximum degree of undercooling can be determined from

$$\Delta T_m = \frac{b}{2\ \mathrm{ProductLog}\left(y\right)} \tag{60}$$

where

$$y = b\left(\frac{\pi\, z\, N_s\, L_e}{c}\right)^{1/2}\left(\frac{2\, D^3\, \beta^3}{B\, Q^3}\right)^{1/4} \quad (61)$$

The ProductLog[y] = x is the Lambert function[3], also is called the omega function and it is graphically shown in Figure 6. This function is used to solve equation of the type of $y = xe^x$. Its exact values can be easily calculated using the instruction of the ProductLog[y] in the Mathematica™ programme. In our analysis typical values of variable y are situated within boundaries from 0.03 to 500, and in case if we cannot use Mathematica programme its value can be calculated by means of elementary mathematics with an accuracy higher than 99% using the following equations:

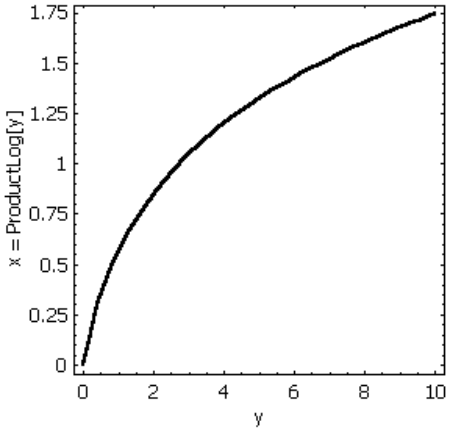

Fig. 6. *Graphic representation of the ProductLog[y] function for $y \geq 0$*

– for $0.03 \leq y \leq 1$ range $\quad x = \dfrac{0.232541y}{-0.03066y^2 + 0.204476y + 0.235837}$;

– for $1 \leq y \leq 5$ range $\quad x = \log(0.0855561)y^{0.224539} + 3.03131y^{0.294488}$;

– for $5 \leq y \leq 20$ range $\quad x = \log(0.06014)y^{0.00796} + 3.29565y^{0.135821}$;

– for $20 \leq y \leq 50$ range $\quad x = \log(0.038806)y^{-0.04997} + 3.59672y^{0.110107}$;

– for $20 \leq y \leq 500$ $\quad x = \log(0.059427)y^{-0.34418} + 2.03579y^{0.144835}$.

From Eqs. (57) and (60) N can be given by

$$N = \frac{N_s}{\exp\left[2\ \text{ProductLog}(y)\right]} \quad (62)$$

In metallographic determinations, the area density of graphite nodules N_F is commonly measured at a given micro-section. In addition, in ductile iron the graphite nodules are cha-

[3] See http://mathworld.wolfram.com./LambertW-function.html.

racterized by Raleigh distributions [12]. In this case the volumetric nodule count (N) can be related to the area nodule count (N_F) using the Wiencek equation [13]

$$N_F = \left(f_{gr} N^2 \right)^{1/3} \tag{63}$$

where f_{gr} is the volume fraction of graphite in eutectic, $f_{gr} = 0.11$.

According to the literature, the nodule count N_F is influenced by the chemical composition and the superheat temperature and time [14]. Yet, in the industrial practice, a drastic increase in nodule counts is usually obtained by the introduction of inoculants. In this case, the nodule count depends on the type of inoculant, quantity and granulation, Mg treatment and inoculation temperature, and the time after inoculation [14]. Also, it is well known that an increase in the cooling rates causes a radical increase in the nodule count in castings.

From Eqs. (60) and (61) it can be seen that among the various factors that influence the final nodule count are:

– The diffusion coefficient of carbon in austenite, D depends on the actual temperature and chemical composition of the austenite. The effect of Si, Mn and P on D is not considered in this work as there is not enough information available in the literature. An expression for the diffusion coefficient of carbon in austenite has been published [15]

$$D = \left(0.00453 + \frac{3.33957}{T} \right) \exp\left[15176.273 \left(0.0002221 - \frac{1}{T} \right) \right], \text{cm}^2/\text{s} \tag{64}$$

During the eutectic transformation, the temperature, T ranges from 1373.3 to 1423.3 K, so the effective D values ranges from $3.2 \cdot 10^{-6}$ to $4.6 \cdot 10^{-6}$ cm^2/s. Therefore, an average D value of $3.9 \cdot 10^{-6}$ cm^2/s can be used without introducing significant error. In general, as D increases, the nodule count decreases as predicted by Eqs. (61)–(11), (also see Fig. 7).

– Nucleation susceptibilities. Depending on the graphite nucleation susceptibilities in ductile cast iron at a given cooling rate, various nodule counts can be achieved. The nucleation susceptibilities of cast iron (Tab. 1) are characterized by N_s and b. These coefficients (see Tab. 4, Part II) depend on the chemical composition, spheroidization practice, inoculation, and holding time of bath and temperature.

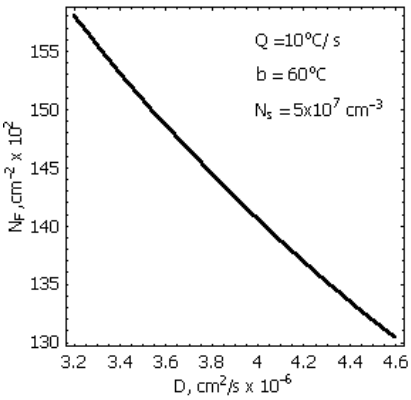

Fig. 7. *Influence of the diffusion coefficient for carbon in austenite on the nodule count; L_e = 2028.8 J/cm^3; c = 5.95 J/(cm$^{3.o}$C); β = 0.00155^{o}C^{-1}; C = 3.71%, Si = 2.77%, P = 0.0234%; T_i = 1300^{o}C; D = = 3.9 10^{-6}cm^2/s (rest of data see Tab. 1)*

Table 1. Physical-chemical data for nodular cast iron

Latent heat of graphite eutectic	$L_e = 2028.8\ \mathrm{J\cdot cm^{-3}}$
Specific heat of the cast iron	$c = 5.95\ \mathrm{J\cdot cm^{-3}.^oC}$
Coefficient of heat accumulation by the mould material	$a = 0.1\ \mathrm{J\cdot cm^{-2}\cdot s^{-1/2}.\ ^oC}$
Diffusion coefficient of carbon in austenite	$D = 3.9 \cdot 10^{-6}\ \mathrm{cm^2\cdot s^{-1}}$
Coefficient	$\beta = 0.00155^oC^{-1}$
Equilibrium temperature of the graphite eutectic	$T_s = 1154 + 5.25Si - 14.88P$
Cementite eutectic formation temperature	$T_c = 1130.56 + 4.06(C - 3.33Si - 12.58P),\ ^oC$
$\Delta T_{sc} = T_s - T_c$	$\Delta T_{sc} = 23.34 - 4.06C + 18.80Si + 36.29P,\ ^oC$
Eutectic density	$\rho_e = 0.926\rho_\gamma + 0.074\ \rho_{gr},\ \mathrm{g\cdot cm^{-3}}$
Austenite density	$\rho_\gamma = 7.51\ \mathrm{g\cdot cm^{-3}}$
Graphite density	$\rho_{gr} = 2.22\ \mathrm{g\cdot cm^{-3}}$
Melt density	$\rho_l = 7.1\ \mathrm{g\cdot cm^{-3}}$
Average temperature of the metal just after pouring in the mold cavity	$T_i = 1250^oC$

The influence of the nucleation coefficients on the nodule count is shown in Figure 8. The calculations made for nodule count were based on Eqs. (61)–(63). From Figure 8, it is apparent that the nodule count increases when b decreases and N_s increases. In addition, it is well known [11] that for given cooling rate prolonged bath holding time leads to reduction in N_s and to an increase in b – parameter. Consequently, prolonged bath holding time leads to a reduction in the nodule count.

– According to Eq. (15) the cooling rate increases as the ability of the mold to absorb heat a increases and as the casting modulus M decreases. The cooling rate is also dependent on the B parameter (Eq. 14), and hence on the initial temperature T_i of the cast iron just after pouring into the mould. It also depends on the equilibrium eutectic temperature T_s and the specific heat c (Eq. (15). Figure 9 shows the effect of B and of the a/M ratios on the cooling rate at the onset of eutectic solidification. A schematic diagram showing the role of various technological factors on the nodule count in ductile cast iron is given in Figure 10.

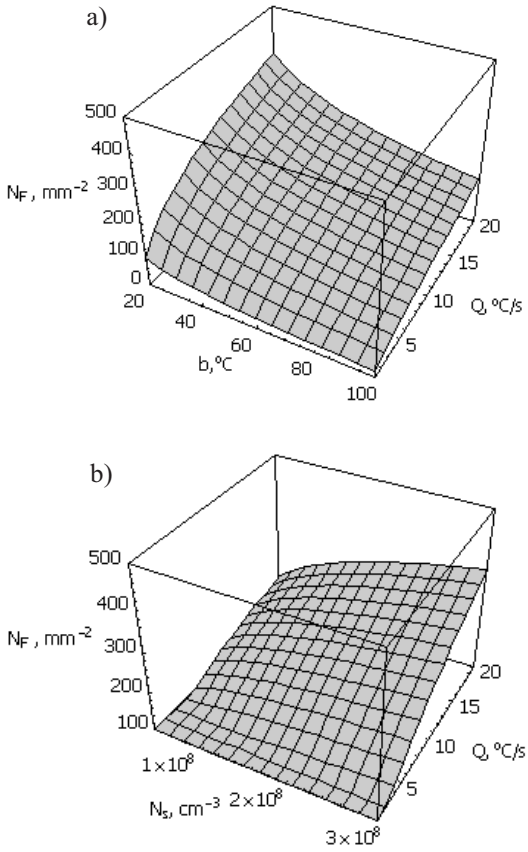

Fig. 8. *Influence of the nucleation coefficient on the nodule count: a) $N_s = 5\cdot10^7$ cm^{-3}; b) b = 60°C (rest of data see Fig. 7)*

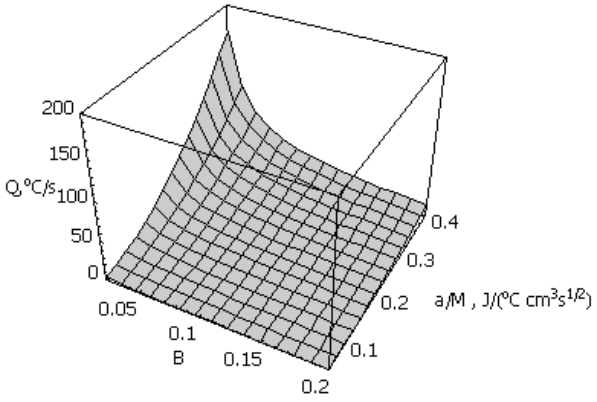

Fig. 9. *Effect of B (T_i, T_s) and a/M ratio on the cooling rate Q*

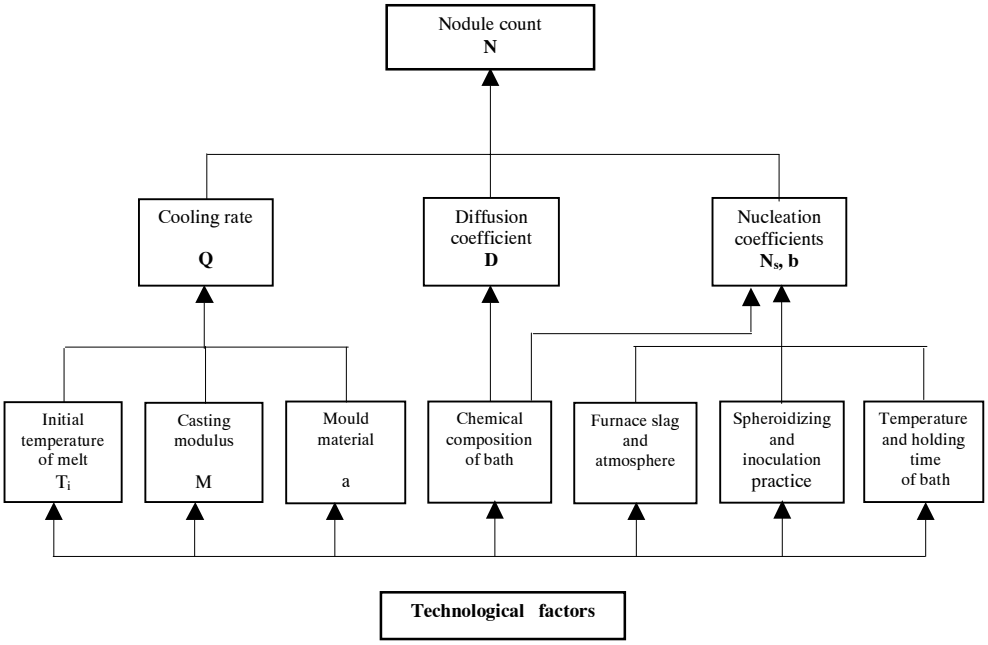

Fig. 10. *Effect of technological factors on the nodule count in ductile cast iron*

4. CHILLING TENDENCY

Since $\Delta T_m = T_s - T_m$, a plot of the function $T_m = f(Q)$ using Eqs. (60) and (61) is given in Figure 11. From this figure, it is found that the minimum temperature for the solidification of the graphite eutectic T_m levels with the temperature T_c when the cooling rate, $Q = Q_{cr}$ and $\Delta T_m = T_s - T_c = \Delta T_{sc}$, so below T_c, the solidification of cementite eutectic begins. By taking into account this condition into Eqs. (60) and (61) and using Eq. (15) an expression is derived for the critical casting modulus $M_{cr} = (V/F)_{cr}$ below which a chill is likely to develop in castings

$$M_{cr} = p_{cr}\ \mathrm{CT} \tag{65}$$

where the coefficient p_{cr} includes the parameters (a, z, B T_s) related to the cast iron cooling rates[4)]

$$p_{cr} = a \left(\frac{T_s^3}{4\,\pi^5\,\beta\,z^2\,B^2\,L_e^2\,c^4} \right)^{1/6} \tag{66}$$

[4)] Influence of L_e and c can be neglected.

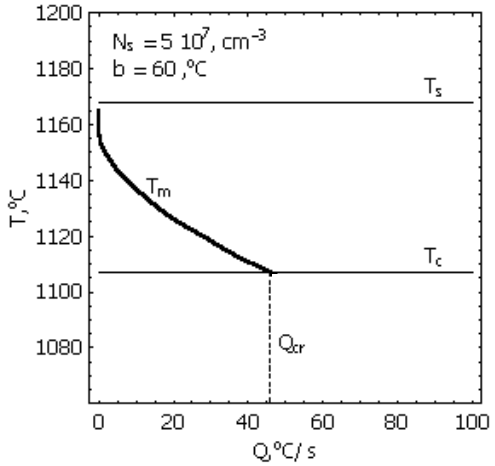

Fig. 11. *Influence of the cooling rate Q on the minimal solidification temperature T_m for graphite eutectic (rest of data see Fig. 7)*

CT is the chilling tendency for ductile cast iron

$$\mathrm{CT} = \frac{1}{D^{1/2}}\left[\frac{1}{N_s\ \beta\ \Delta T_{sc}^2}\exp\left(\frac{b}{\Delta T_{sc}}\right)\right]^{1/3} \tag{67}$$

From Eqs. (57) and (67), for $\Delta T_m = \Delta T_{sc}$, CT can be simplified to

$$\mathrm{CT} = \frac{1}{D^{1/2}}\left(\frac{1}{N\ \beta\ \Delta T_{sc}^2}\right)^{1/3} \tag{68}$$

Typical CT values range from 0.8 to 1.2 $s^{1/2} / {}^{o}C^{1/3}$. The influence of the various terms on CT, (Eq. (68)) can be summarized as:

– Diffusion coefficient, as D increases, CT decreases.
– The temperature range $\Delta T_{sc} = T_s - T_c$, depends on the chemical composition as

$$\Delta T_{sc} = 23.34 - 4.07\mathrm{C} + 18.80\mathrm{Si} + 36.29\mathrm{P},\ {}^{o}\mathrm{C} \tag{69}$$

In particular, carbon reduces ΔT_{sc} while silicon expends it (Fig. 12a). The effect of this range on CT is shown in Figure 12b. Notice from this figure that CT decreases with increasing ΔT_{sc} ranges.

– The Nucleation susceptibilities of graphite depends on the resultant values of N_s and b (see previous section). In particular, CT increases with increasing b and decreasing N_s (Fig. 13).

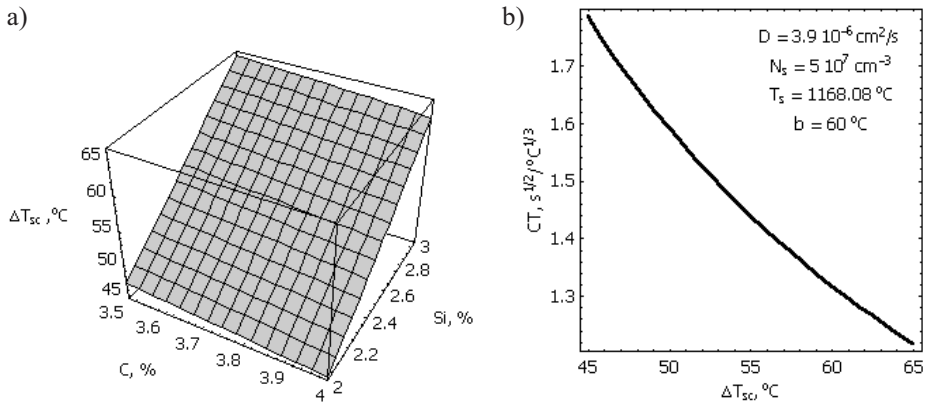

Fig. 12. *Influence of carbon and silicon on: a) ΔT_{sc}; b) ΔT_{sc} on the chilling tendency CT*

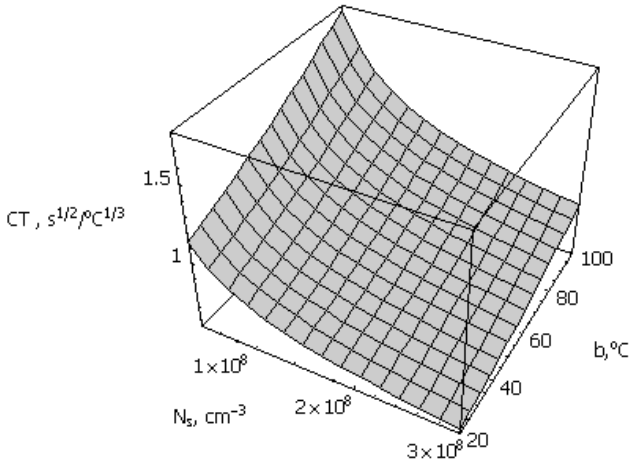

Fig. 13. *Influence of N_s and b on the chilling tendency of ductile cast iron; $\Delta T_{sc} = 60^oC$ (rest of data see Fig. 7)*

5. CHILL

In establishing the chill of cast iron, it is common to implement a set of chill tests on castings, which consist of plates with different wall thicknesses, thus the critical casting modulus can be determined from

$$M_{cr} = \frac{V_{cr}}{F_{cr}} \tag{70}$$

where V_{cr} and F_{cr} are chilled volume and surface area of casting.

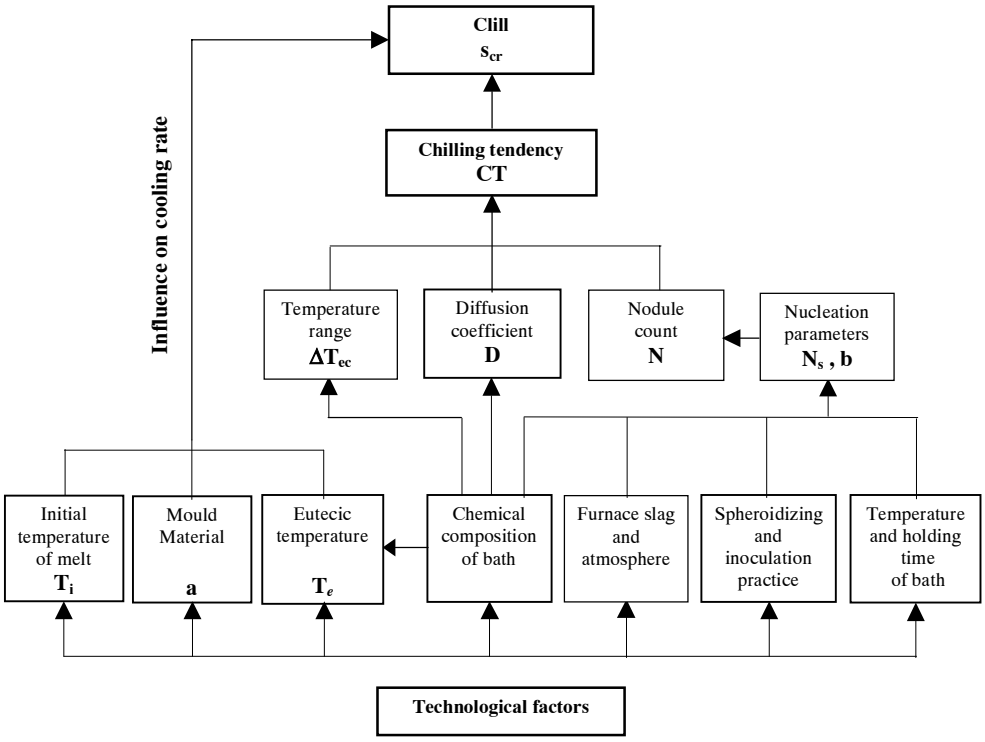

Fig. 14. *Effect of technological factors on the chill and chilling tendency of ductile iron*

For plates with wall thickness, s and lengths and widths which easily exceed s, M_{cr} = $= V_{cr}/F_{cr} = (s_{cr} F_{cr})/(2 F_{cr})$, and the critical wall thickness s_{cr} below which the chill forms is

$$s_{cr} = 2 M_{cr} \tag{71}$$

and after using Eq. (65)

$$s_{cr} = 2 p_{cr} \text{ CT} \tag{72}$$

From Eqs. (66), (67) and (72) results a diagram showing the influence of technological factors on chilling tendency CT and the chill of ductile cast iron is shown in Figure 14.

6. CONCLUSIONS

A theoretical analysis is proposed for the solidification of ductile cast iron which allows to predict nodule counts based only on the knowledge of cooling rates and chemical composition, the initial temperature of the metal just after pouring into the mould, the diffu-

sion coefficient of carbon in austenite and the graphite nucleation coefficients. From the proposed theory, expressions are derived for the chilling tendency and chill of cast iron.

A summary of the present analysis on the nodule count of cast iron indicates that it depends on:

- The chemical composition of the cast, through D, N_s, and b.
- The inoculation practice, the bath superheating temperature and time, furnace slag and atmosphere, through N_s and b.
- Cooling rate, through M, a and B.

The chilling tendency CT of the nodular cast iron depends on:

- Chemical composition through D, ΔT_{sc}, N_s, and b,
- Inoculation and spheroidization practice, superheat temperature and time, as well as furnace slag and atmosphere through N_s and b.

In addition, the chill of the nodular cast iron is related to cooling rate Q and CT.

REFERENCES

[1] *Jincheng Liu, Elliot R.*: The influence of cast structure on the austempering of ductile iron. International Journal of cast Metals Researches, 11 (1999), p. 407

[2] *Lesoult G., Castro M., Lacaze J.*: Solidification of Spheroidal Graphite Cast Iron: III Microsegregation related effects. Acta Materialia, 47 (1999), p. 3779

[3] *Achmadabadi M.N., Niyama E., Ohide T.*: Structural control of 1% Mn aided by modeling of micro-segregation. Transactions of the American Foundrymans Society, 97 (1994), p. 269

[4] *Javaid A., Thompson J., Davis K.G.*: Critical conditions for obtaining carbide – free microstrucutre in thin-wall ductile iron. AFS Transactions, 102 (2002), p. 889

[5] *Javaid A., Thompson J., Sahoo M., Davis K.G.*: Factors affecting formation of carbides in thin-wll DI castings, AFS Transactions, 99 (1999), p. 441

[6] *Fraś E., Lopez H.*: Generation of International Pressure During Solidification of Eutectic Cast Iron. Transactions of the American Foundryman Society, 102 (1994), p. 597

[7] *Fraś E., Podrzucki C.*: Inoculated Cast Iron. AGH, Cracov, 1981

[8] *Venugopalan D.*: A Kinetic Model of the $\gamma \rightarrow \alpha$ + Gr Eutectoid Transformation in Spheroidal Graphite Cast Iron. Metallurgical and Materials Transactions, 21 A (1990), p. 913

[9] *Chvorinov N.*: Theorie der Erstarrung von Gusstűcken. Die Giesserei (1940) 27, p. 10

[10] *Fras E., Lopez H.*: A theoretical analysis of the chilling suspectibility of hypoeutectic Fe-C alloys. Acta Metallurgica and Materialia, 41 (1993) 12, p. 3575

[11] *Fras E., Górny M., Lopez H., Tartera J.*: Nucleation and grains density in grey cast iron. A theoretical model and experimental verification. International Journal of Cast Metals Research, 16 (2003), pp. 99÷104

[12] *Wojnar L.*: Effect of graphite size and distribution on fracture and fractography of ferritic nodular cast iron. Acta Stereologica, 5/2 (1986), p. 319

[13] *Wiencek K., Ryś J.*: The estimation of Fe_3C particle density in steel by simple counting measurements made in plan sections. Materialas Engineering (1998) 3, p. 396

[14] *Merchant H.D.*: Solidification of Cast Iron, Recent Research on Cast iron. Gordon and Breach, Science Publishers, New-York, 1968

[15] *Agren J.*: A revised expression for the diffusivity of carbon in binary Fe-C austenite. Scripta Metallurgica, 20 (1986), p. 1507

Received
March 2005